Experimental report

13/02/2019

Proposal: **7-05-476** **Council:** 4/2017

Title: The role of inter-adsorbate interactions and adsorption geometry in surface diffusion

Research area: Physics

This proposal is a new proposal

Main proposer: **Anton TAMTOEGL**

Experimental team: Peter FOUQUET
Anton TAMTOEGL

Local contacts: Peter FOUQUET
Michael Marek KOZA

Samples: Graphite
Triphenylphosphine P(C6H5)3
Deuterated triphenylphosphine P(C6D5)3

Instrument	Requested days	Allocated days	From	To
IN6	6	0		
IN11	10	7	31/05/2018	07/06/2018
IN6-SHARP	0	4	28/03/2018	02/04/2018

Abstract:

In previous neutron scattering experiments, we have studied and characterized the diffusive behaviour of polyciclic hydrocarbons (PAH) adsorbed on exfoliated graphite substrates extensively. In the proposed experiment we would like to study the diffusion of triphenylphosphine (PPh3) on graphite. In doing so we attempt to characterise the role of adsorption geometry and lateral interactions between adsorbates in surface diffusion. This is based on the fact that PPh3 exhibits a completely different adsorption geometry compared to PAHs as well as due to its dipole moment which should give rise to a strong coverage dependence of the diffusive process.

The role of inter-adsorbate interactions and adsorption geometry in surface diffusion

Anton Tamtögl,*,† Marco Sacchi,‡ Michael M. Koza,¶ and Peter Fouquet¶

†*Institute of Experimental Physics, Graz University of Technology, Graz, Austria*
‡*Department of Chemistry, University of Surrey, GU2 7XH, Guildford, United Kingdom*
¶*Institut Laue-Langevin, 71 Avenue des Martyrs, 38000 Grenoble, France*

E-mail: tamtoegl@gmail.com

1 Scientific background

Triphenylphosphine - $P(C_6H_5)_3$ - is an important ligand for organic, organometallic, and nanoparticle synthesis[1,2] and shows a complex self-assembly behaviour on Au(111)[2]. However, in contrast to other organic compounds, the surface chemistry of PPh_3 has to date gone almost completely unexamined[3]. Here we present an experimental and computational study of the diffusion of triphenylphosphine (PPh_3) on exfoliated graphite.

While the diffusion of polycyclic hydrocarbons (PAH) on graphite has been subject to several recent studies[4–6], the dynamics of other species on graphite is relatively unexplored. Unlike previous studies of flat PAHs on graphite the PPh_3 molecule exhibits a completely different geometry: PPh_3 is pyramidal with a chiral propeller-like arrangement of the three phenyl rings[7]. On hexagonal metal surfaces PPh_3 molecules adsorb in an upright fashion in contrast to PAHs which typically adsorb in a planar configuration. This adsorption geometry gives rise to a rather dense packing structure on the surface[2,8]. Hence in comparison to the dynamics of PAHs on graphite the question arises how the adsorption geometry influences the diffusive process.

Moreover, while "flat" PAHs do not exhibit a dipole moment, PPh_3 has a dipole moment of about 1.4 Debye[1], similar to water. Due to this dipole moment possible lateral interactions between the diffusing adsorbates may play an important role. Interactions among the adsorbates such as dipole forces give rise to a deviation in the QENS broadening as a function of momentum transfer $\mathbf{Q}$. This behaviour has been predicted and described using analytical models already in 1959 by de Gennes[9]. However, while it has been studied and observed in liquids, the role of adsorbate interactions for the diffusion on surfaces has been hardly covered by experiment[10].

Apart from the fundamental interest, the diffusion of PPh_3 on graphite is of great importance for applications. For example, phosphorus doped graphene nanosheets can be prepared via annealing of graphene oxide in the presence of PPh_3. These nanosheets show excellent NH_3 sensing ability at room temperature[11]. Moreover, it was shown that the preparation of PPh_3 modified graphene quantum dots gives rise to a high quantum yield and excellent stability[12]. In a wider context, the diffusivity of triphenyl compounds is also of paramount importance for medical purposes: Triphenylbismuth and triphenylantimony are currently under investigation as contrast agents for magnetic resonance imaging[13] while triphenylphosphine has recently been incorporated in a macromolecule that can be used as a vehicle for mitochondrial drug delivery[14].

2 Experimental details

2.1 Sample preparation

As a substrate we used exfoliated compressed graphite, *Papyex*, which exhibits an effective surface area of about 25 m^2 g^{-1} and retains a sufficiently low defect density[15,16]. Due to its high specific adsorption surface area it is widely used for adsorption measurements. We further exploit the fact that, exfoliated graphite samples exhibit a preferential orientation of the basal plane surfaces and oriented those parallel to the scattering plane of the neutrons. Each sample was prepared with 12-13 g of Papyex exfoliated graphite of grade N998 (> 99.8% C, Carbone Lorraine, Gennevilliers, France). The prepared exfoliated graphite disks were heated to 973 K under vacuum before transferring them into a cylindrical aluminium sample cartridge. The amount of powder PPh_3 ($C_{18}H_{15}P$ and $C_{18}D_{15}P$), required to reach the corresponding ML coverage, was weighed using a fine balance and then added to the graphite disks. At monolayer coverage the area occupied by one PPh_3 molecule corresponds to $\Sigma = 63$ Å^2 (based on[2]). Finally, the aluminium sample holders were hermetically sealed using a lid with a steel knife-edge. The samples were then heated in an evacuated furnace to 400 °C to sublimate the PPh_3 and promote its adsorption in the whole volume of the sample.

2.2 Instrumental details

The measurements were carried out at the IN6 time-of-flight (TOF) neutron spectrometer and the IN11 neutron spin-echo (NSE) spectrometer of the ILL[17]. The incoming neutron wavelengths were set to 5.12 Å and 5.5 Å, respectively, with energy resolutions at full width at half maximum of 70 μeV (IN6) and 1 μeV (IN11). Neutron scattering TOF spectra of $P(C_6H_5)_3$/graphite were obtained over a large temperatures region, ranging from 2 K to 500 K (at 0.2 ML and 0.5 ML PPh_3 coverages). Neutron spin-echo measurements of $P(C_6D_5)_3$/graphite were performed over the same thermal range at 0.5 ML and 0.9 ML coverages, respectively.

The TOF spectra were converted to scattering functions, $S(Q, \Delta E)$, where $Q = |\mathbf{Q}| = |\mathbf{k_f} - \mathbf{k_i}|$ is the momentum transfer and $\Delta E = E_f - E_i$ is the energy transfer. From

NSE measurements the normalised intermediate scattering function $I(Q,t)/I(Q,0)$ was extracted[18,19] which is related to the scattering function $S(Q,\Delta E)$ via a Fourier transform in time.

3 Results

3.1 Neutron scattering results

Neutron TOF scattering The experimentally measured scattering function $S(Q,\Delta E)$ (normalised by Vanadium) was fitted using a convolution of the resolution function of the neutron TOF spectrometer $S_{res}(Q,\Delta E)$ (scattering function of PPh_3/graphite measured at base temperature) with an elastic term $I_{el}(Q)\delta(\Delta E)$, the quasi-elastic contribution $S_{inc}(Q,\Delta E)$ and a linear background:

$$S(Q,\Delta E) = S_{res}(Q,\Delta E) \otimes \left[I_{el}(Q)\delta(\Delta E) + A(Q)\frac{1}{2\pi}\frac{\Gamma(Q)}{[\Gamma(Q)]^2+\Delta E^2} + C(Q) \right]. \quad (1)$$

Here, δ represents the Dirac delta and the quasi-elastic broadening is modelled by a Lorentzian function, where $I_{el}(Q)$ is the intensity of the elastic scattering and $A(Q)$ is the intensity of the quasi-elastic scattering. $\Gamma(Q)$ is the half width at half maximum (HWHM) of the Lorentzian.

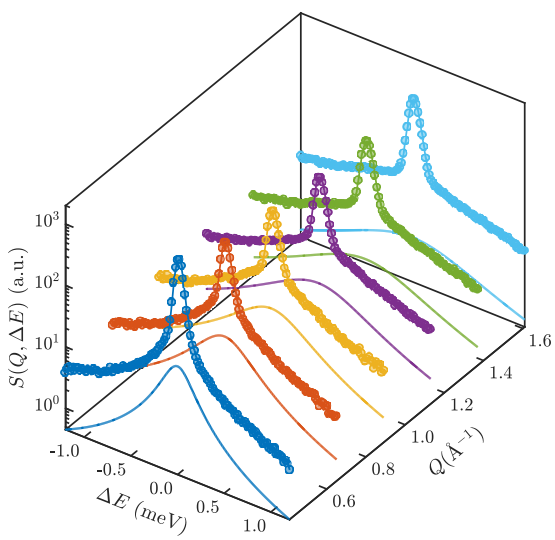

Figure 1: Several dynamic scattering functions $S(Q,\Delta E)$ (symbols) as extracted from neutron TOF data for exfoliated graphite covered by 0.5 ML of PPh_3. The solid lines show the fitted quasi-elastic Lorentzian broadenings obtained by fitting (1).

Neutron spin-echo scattering The intermediate-scattering function (ISF) obtained from the spin-echo measurements was fitted using a stretched exponential decay function

$$I(Q,t) = y_0 + (1-y_0)\exp\left[-\left(\frac{t}{\tau}\right)^{\beta}\right] \quad (2)$$

where y_0 is the fraction of static signal and β is the stretching exponent ($\beta \leq 1$, with $\beta = 1$ for a single exponential decay).

Figure 1 shows several dynamic scattering functions

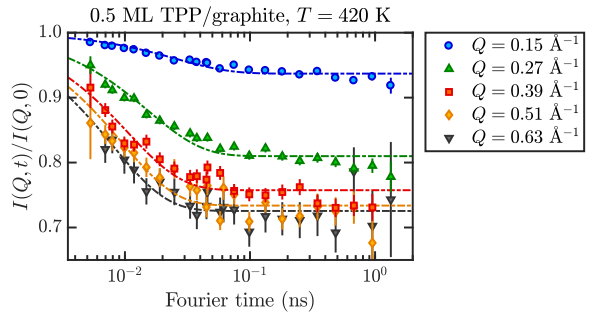

Figure 2: $I(Q,t)/I(Q,0)$ for the 0.5 ML data, fitted with a single exponential fit ((2) with $\beta = 1$, dash-dotted lines)

$S(Q,\Delta E)$ (symbols) as extracted from the neutron TOF data for exfoliated graphite covered by 0.5 ML of PPh_3. The solid lines show the fitted quasi-elastic Lorentzian broadenings based on fitting (1).

Figure 2 shows two NSE measurements. They are best described by a single exponential decay as shown in the upper panel of Figure 2. Note however, that at at a sample temperature of 350 K, in particular the low Q data at 0.9 ML coverage is better described by a fit with $\beta < 1$ (lower panel of Figure 2). The effect becomes less pronounced at 420 K whereas at 500 K it tends to be well described with a single exponential fit again.

3.2 Temperature dependence

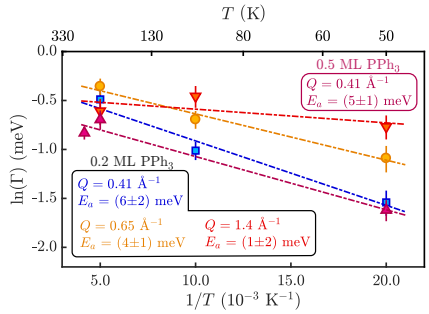

(a) Arrhenius plot of the low temperature phase for the neutron TOF scattering measurements.

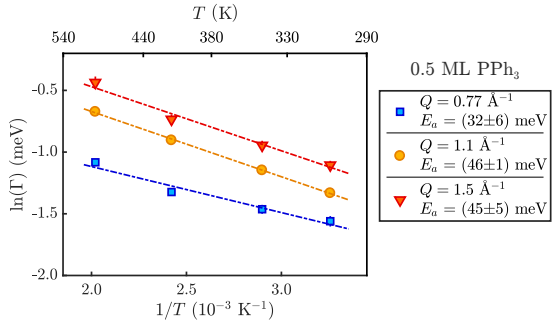

(b) Arrhenius plot of the high temperature phase for several different momentum transfers Q at a molecular coverage of 0.5 ML.

Figure 3: Arrhenius plots of the broadening extracted from the neutron TOF measurements of PPh_3/graphite.

The temperature dependence shows a clear trend which is similar for both NSE and neutron TOF and all three cover-

ages. The extracted broadening is basically flat up to about 300 K (as far as it can be resolved) and becomes then an activated (translational) motion at around 300-350 K. The low temperature phase is likely to be dominated by rotational motion (see subsection 3.3) while the high temperature phase is dominated by translational motion with an activation barrier of about 40 meV. In particular at smaller Q-values the Arrhenius plot shows a minute coverage dependence with E_a increasing with increasing molecular coverage.

3.3 Momentum transfer dependence

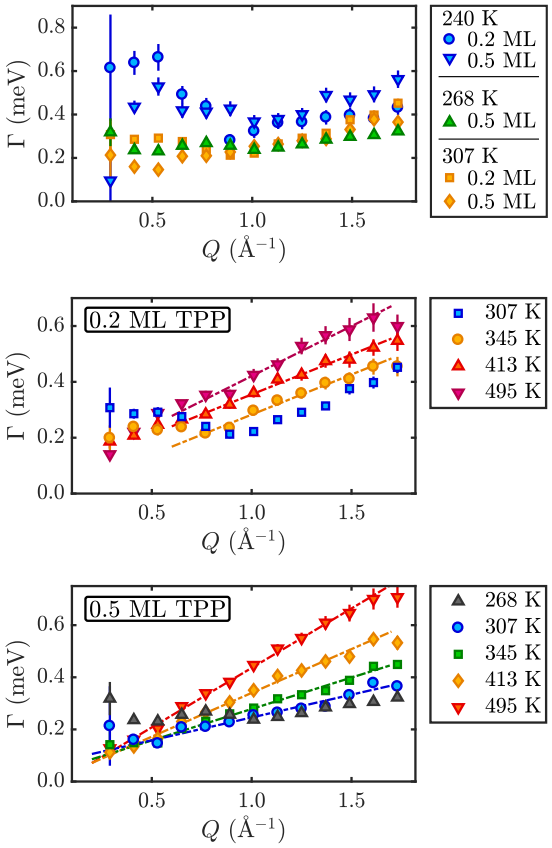

Figure 4: Extracted quasi-elastic broadening $\Gamma(Q)$ for 0.2 and 0.5 ML PPh_3 at several temperatures versus momentum transfer Q. The broadening shows only a weak momentum transfer dependence at low temperature turning into a linear dependence upon Q at higher temperatures as illustrated by the dash-dotted lines.

Again the data is similar for both NSE and neutron TOF and at all three coverages, being more or less constant up to about 300 K which clearly points towards rotational motion in the low temperature phase. In Figure 4 the broadening shows only a weak momentum transfer dependence at low temperature turning into a linear relationship with Q with increasing temperature (see the bottom panel in Figure 5 for a comparison of the NSE and TOF data in the high temperature phase). The broadening at low temperature could be caused by rotations of the molecule and flapping motions of the phenyl groups (preliminary forcefield molecular dynamics simulations suggest that this type of motion is already active at much lower temperatures compared to the translationsl motion) which then gradually turns into diffusive motion across the surface with increasing temperature.

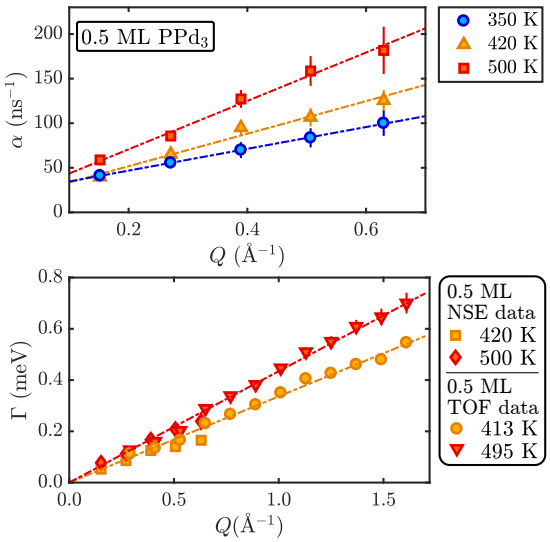

Figure 5: Dephasing rate $\alpha = 1/\tau$ versus momentum transfer Q as extracted from the neutron spin-echo measurements for deuterated PPh_3 ($P(C_6D_5)_3$) at different temperatures. The bottom panel shows a comparison of the SE data with the broadening extracted from the TOF data.

References

1. Allen, D. W. In *Organophosphorus Chemistry*; Allen, D. W., Loakes, D. *et al.* , Eds.; Royal Society of Chemistry: Cambridge, 2016; Vol. 45; pp 1–50, 00000.
2. Jewell, A. D.; Sykes, E. C. H. *et al. ACS Nano* **2012**, *6*, 3545–3552, 00018.
3. Westermark, G.; Kariis, H. *et al. Colloids Surf. A* **1999**, *150*, 31–43, 00023.
4. Calvo-Almazán, I.; Sacchi, M. *et al. J. Phys. Chem. Lett.* **2016**, *7*, 5285–5290.
5. Calvo-Almazán, I.; Bahn, E. *et al. Carbon* **2014**, *79*, 183 – 191.
6. Hedgeland, H.; Fouquet, P. *et al. Nat Phys* **2009**, *5*, 561–564.
7. Ziemer, B.; Rabis, A. *et al. Acta Cryst. C* **2000**, *56*, e58–e59.
8. Steiner, U. B.; Neuenschwander, P. *et al. Langmuir* **1992**, *8*, 90–94.
9. De Gennes, P. *Physica* **1959**, *25*, 825–839, 00577.
10. Lechner, B. A. J.; de Wijn, A. S. *et al. J. Chem. Phys* **2013**, *138*, 194710.
11. Niu, F.; Tao, L.-M. *et al. New J. Chem.* **2014**, *38*, 2269, 00000.
12. Yang, S.; Zhu, C. *et al. RSC Adv.* **2015**, *5*, 33347–33350, 00009.
13. Scharfetter, H.; Gösweiner, C. *et al. Mol. Phys.* **2018**, *0*, 1–9.
14. Khatun, Z.; Choi, Y. S. *et al. Biomacromolecules* **2017**, *18*, 1074–1085.
15. Gilbert, E. P.; Reynolds, P. A. *et al. J. Chem. Soc. Faraday Trans.* **1998**, *94*, 1861–1868.
16. Finkelstein, Y.; Nemirovsky, D. *et al. Physica B Condens Matter* **2000**, *291*, 213 – 218.
17. Tamtögl, A.; Fouquet, P. *et al.* The role of inter-adsorbate interactions and adsorption geometry in surface diffusion. Institut Laue-Langevin (ILL). doi:10.5291/ILL-DATA.7-05-476. 2016.
18. Fouquet, P.; Hedgeland, H. *et al. Z. Phys. Chem* **2010**, *224*, 61–81.
19. Mezei, F. In *Neutron Spin Echo: Proceedings of a Laue-Langevin Institut Workshop Grenoble, October 15–16, 1979*; Mezei, F., Ed.; Springer, 1980; Chapter The principles of neutron spin echo, pp 1–26.